# Pathways for Photoinduced Charge Separation and Recombination at Donor−Acceptor Heterojunctions: The Case of Oligophenylenevinylene−Perylene Bisimide Complexes

**A. Burquel, V. Lemaur, D. Beljonne, R. Lazzaroni, and J. Cornil***

*Laboratory for Chemistry of Novel Materials, University of Mons-Hainaut, Place du Parc 20, B-7000 Mons, Belgium*

*Received: October 7, 2005; In Final Form: November 25, 2005*

Semiempirical Hartree−Fock techniques have been applied to assess the molecular parameters governing the efficiency of photoinduced charge generation and recombination processes in donor/acceptor complexes involving a three-ring oligophenylenevinylene as donor and perylene bisimide as acceptor. The corresponding rates have been estimated in the framework of the Marcus−Levich−Jortner formalism for different geometries of the complexes. The results indicate that dissociation pathways involving the lowest two charge transfer excited states contribute significantly to the dynamics of the whole process. The rates are found to be strongly sensitive to the relative position of the donor and acceptor units and can be rationalized in terms of symmetry arguments applied to relevant electronic levels.

## 1. Introduction

Organic-based solar cells attract considerable interest as a new alternative source of renewable energy. The use of organic materials offers several advantages compared to their inorganic counterparts, in particular the modulation of their electronic properties by molecular engineering, the ease of processing, as well as the low manufacturing costs. Solar cells are designed for converting the light irradiated by the sun into electrical charges to produce a current in an external circuit. The typical architecture of such a device consists of an organic layer sandwiched between two electrodes of different nature; the organic layer incorporates an electron donating material (D), which exhibits a low ionization potential and an electron accepting unit (A) characterized by a high electron affinity; a great deal of interest has been for instance dedicated to devices based on poly(*p*-phenylenevinylene) (PPV) chains as the donor and fullerene ($C_{60}$) as the acceptor.[1]

The mechanism for light conversion into charges involves four subsequent steps (Figure 1): (i) Light is absorbed by the donor and/or the acceptor to generate intramolecular electron−hole pairs; in a simple one-electron picture, an electron is promoted from the HOMO (highest occupied molecular orbital) of the excited molecule to its LUMO (lowest unoccupied molecular orbital) level. These excitations display a binding energy largely exceeding *kT*, thereby hindering efficient charge generation in single-component devices.[2] (ii) The excitations migrate toward the interface between the donor and the acceptor. (iii) At the interface, when the donor [acceptor] is initially excited, the electron [hole] lying in the LUMO of the donor [HOMO of the acceptor] is transferred to the LUMO of the acceptor [HOMO of the donor] following a photoinduced electron [hole] transfer process; this ultimately yields a charge separated state (with a positive charge on the donor and a negative charge on the acceptor) (see Figure 1). (iv) The generated charges that escape their mutual Coulomb attraction propagate through the organic layer to the electrodes where they are collected.

These four processes have to be optimized to guarantee a high yield of light conversion. The best values reported to date for polymer-based solar cells approach 5%[3] and start competing with devices based on amorphous silicon. However, there is still room for improvement in view of the current limitations of organic-based solar cells. The main drawbacks related to the previously described steps are in the same order: (i) The poor match between the spectral range for absorption in most organic conjugated systems and the solar emission spectrum requires the synthesis of low-band gap materials combining high processability, high absorption coefficients, and good charge transport properties.[4−8] (ii) The exciton diffusion range is quite limited, on the order of 10 nm,[9] and thus a very fine dispersion between the two components is required to promote a large interface area. (iii) The electron and the hole can be simultaneously transferred from the donor to the acceptor or vice versa, thus giving rise to an energy transfer instead of a charge transfer.[10] (iv) The charges have to escape from their mutual Coulomb attraction, estimated to be on the order of a few tenths of an electronvolt;[11] this cannot simply occur upon thermal activation or under the influence of the electric field generated across the organic layer.

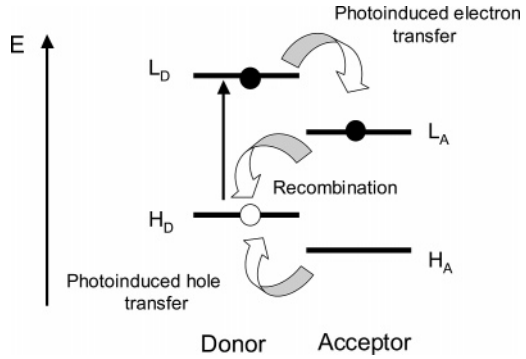


**Figure 1.** Illustration of the photoinduced electron/hole transfer and charge recombination processes in a donor/acceptor pair (H = HOMO; L = LUMO; D = donor; A = acceptor).

The generation of free charge carriers also competes with a recombination mechanism in which the electron in the LUMO level of the acceptor is transferred back to the HOMO level of

10.1021/jp055719d CCC: $33.50 
Published on Web 02/09/2006

the donor; the system thus returns to the ground state without generating any charge. It is thus highly desirable to understand the nature of the molecular parameters controlling charge generation versus charge recombination rates to design the best matching partners and the best supramolecular organizations, and the holes [electrons] have to find a continuous path within the donor [acceptor] phase to reach the electrodes, thus pointing once again to the key role played by the morphology of the blends.

This paper addresses the issue of photoinduced charge generation versus charge recombination in organic solar cells. In this context, we have recently developed a theoretical approach based on semiempirical Hartree−Fock techniques to estimate the amplitude of the various parameters controlling the transfer rates for charge generation and recombination in donor/acceptor complexes in the framework of the Marcus−Levich−Jortner formalism.[11] This approach is applied here to model complexes involving a three-ring phenylenevinylene oligomer (PPV3) as donor and a bisimide molecule (PBI) as acceptor (see chemical structures in Figure 2). This study is motivated by the fact that several model systems based on PPV-related segments and bisimide derivatives have been recently synthesized to shed light into the dynamics of the charge generation and recombination processes.[12−14] In these studies, the donor and acceptor units are systematically linked covalently[12,14] or through H-bonds[13] to build a single entity directly amenable to experimental characterization in solution. The model structures considered here in a first stage do not incorporate the spacing unit, which can sometimes play a crucial role in determining the transfer rate, thus making the analysis more complex.

## 2. Theoretical Methodology

The theoretical approach used here is similar to that described extensively in ref 11 and is summarized hereafter. The rates of the charge generation and recombination processes have been estimated with the Marcus−Levich−Jortner formalism as ref 15:

$$k = \left(\frac{4\pi^2}{h}\right) V_{RP}{}^2 \left(\frac{1}{\sqrt{4\pi\lambda_S kT}}\right) \sum_{\nu'} \exp(-S)\frac{S^{\nu'}}{\nu'!} \times \exp\left(\frac{-(\Delta G^\circ + \lambda_S + \nu'\hbar\langle\omega\rangle)^2}{4\lambda_S kT}\right) \quad (1)$$

where $\Delta G^\circ$ represents the Gibbs free energy of the reaction, $V_{RP}$ is the electronic coupling between the initial and final states, $\lambda_s$ is the reorganization energy of the surrounding medium. This formalism treats at the quantum-mechanical level a single effective mode with an energy $\hbar\omega$ (set here equal to 0.2 eV, i.e., the typical energy of a stretching mode in a conjugated backbone) to depict its possible role in assisting the transfer by tunneling effects across the potential energy barrier. $S$ is the Huang−Rhys factor associated with this mode that we directly relate to the internal reorganization energy ($S = \lambda_i/\hbar\omega$). The summation runs over the pathways starting from the vibrational level 0 in the initial state and reaching the vibrational level $\nu'$ in the final state.

$\Delta G^\circ$ has been estimated as the energy difference of the complex between the final and initial states, accounting for the Coulomb attraction between the two units in both states. For a charge generation process initiated from the excited donor ($D^* + A \rightarrow D^+ + A^-$), $\Delta G^\circ_{dis}$ is (when neglecting the entropy contributions):

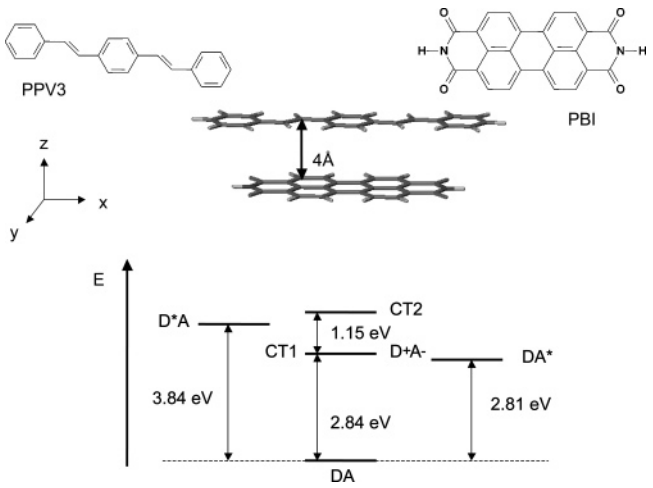


**Figure 2.** Energy diagram of the relevant states in a cofacial dimer built from one three-ring PPV oligomer as donor and one bisimide molecule as acceptor, with an intermolecular distance fixed at 4 Å. The chemical structures of the two compounds are also shown.

$$\Delta G^\circ_{dis} = E^{D^+} + E^{A^-} - E^{D^*} - E^A + \Delta E_{coul} \quad (2)$$

where $E^{D^*}$, $E^{D^+}$, $E^A$, and $E^{A^-}$ represent the total energies of the isolated donor in the equilibrium geometry of the lowest excited state and in the cationic state and those of the isolated acceptor in the equilibrium geometry of the ground state and in the anionic state, respectively. They have been obtained by first optimizing the geometry of the individual molecules in their various redox states with the Austin model 1 (AM1) method[16] coupled to a full configuration interaction (FCI) scheme within an active space built from a few frontier electronic levels.[17] The influence of the dielectric properties of the medium has also been taken into account by coupling in a second step the AM1-CI calculations to the COSMO model,[18] without further geometry optimizations; a static dielectric constant of 3.5, typical of organic-based matrixes, has been used.[19] $\Delta E_{coul}$ is the change in the screened Coulomb interaction between the donor and acceptor units estimated from atomic charges derived from a ZDO (zero differential overlap) analysis based on the AM1-CI/COSMO results. A similar strategy is applied to estimate $\Delta G^\circ$ for the photoinduced hole transfer and charge recombination processes.

The internal part of the reorganization energy $\lambda_i$ is calculated at the AM1-CI level as the average value of $\lambda_{i1}$, corresponding to the difference between the energy of the reactants in the geometry characteristic of the products and that in their equilibrium geometry, and $\lambda_{i2}$, corresponding to the difference between the energy of the products in the geometry characteristic of the reactants and that in their equilibrium geometry.[11,20] The Huang−Rhys factor $S$ is then obtained as $S = \lambda_i/\hbar\omega$.

The external part of the reorganization energy $\lambda_s$ has been estimated from the classical dielectric continuum model initially developed by Marcus for electron transfer reactions between ions in solution.[21] We have modified the original expression in ref 21 by introducing the atomic charges $q_D$ and $q_A$ on the ions, as estimated at the AM1/CI−COSMO level, to account for the molecular topology of the donor and acceptor units:

$$\lambda_S = \frac{1}{8\pi\epsilon_0}\left(\frac{1}{\epsilon_{op}} - \frac{1}{\epsilon_s}\right)\left(\frac{1}{R_D} + \frac{1}{R_A} - 2\sum_D\sum_A \frac{q_D q_A}{r_{DA}}\right) \quad (3)$$

where $\epsilon_s$ is the static dielectric constant of the medium and $\epsilon_{op}$ is the optical dielectric constant taken here to be 2.25. $R_D$ (=3.46 Å) and $R_A$ (=3.45 Å) are the effective radii of the PPV3 and PBI molecules estimated from the surface accessible area of the molecule provided by COSMO.

The electronic coupling $V_{RP}$ is the matrix element of the total Hamiltonian of the system between the initial and final states for a given process. $V_{RP}$ has been estimated with the two-state generalized Mulliken−Hush (GMH) formalism:[22]

$$V_{RP} = \frac{\mu_{RP}\Delta E_{RP}}{\sqrt{(\Delta\mu_{RP})^2 + 4(\mu_{RP})^2}} \quad (4)$$

where $\Delta E_{RP}$ corresponds to the energy difference, $\Delta\mu_{RP}$ is the change in the permanent dipole moment and $\mu_{RP}$ is the transition dipole moment between the initial and final states of the complex; note that $\mu_{RP}$ has to be projected in all cases along the $\Delta\mu_{RP}$ direction, which is mainly oriented along the stacking axis.[23] The use of a two-state model will be fully validated in the next section. The parameters entering into eq 4 have been evaluated using the semiempirical Hartree−Fock INDO (intermediate neglect of differential overlap) method[24] coupled to a single configuration interaction scheme (SCI) involving the highest 40 occupied and lowest 40 unoccupied levels in the active space. When a photoinduced charge transfer initiated from the donor [acceptor] is considered, the intramolecular configurations originating from the HOMO level of the acceptor [donor] are excluded to prevent any exciton delocalization across the donor/acceptor interface because excitons are expected to be localized over a single molecule at room temperature as a result of lattice vibrations. If it is not done, the interaction between the transition dipole moments associated with the lowest excited state of the donor and acceptor leads to a partial delocalization of the excitation over the whole complex and hence overestimated electronic couplings. Another issue to deal with is the fact that INDO/SCI calculations do not take the medium effects into account and hence do not necessarily provide reliable energies for the charge transfer excited states, we have therefore calibrated their position with an electric field to match the results provided by AM1-CI/COSMO calculations; this procedure has been described in details in ref 11.

### 3. Results and Discussion

We have first considered a cofacial dimer built by superimposing the centers of mass of the PPV oligomer (assumed to be fully planar) and the perylene bisimide, with their molecular axes lying parallel to one another and the intermolecular separation set at 4 Å (Figure 2); we stress that the picture derived hereafter holds true for other intermolecular distances. Note that the electronic couplings, and hence the transfer rates, are vanishingly small when the two molecules are coplanar and are not covalently linked, thus rationalizing the choice of a superimposed structure. We report in Figure 2 the energy of the relevant excited states of the dimer in their fully relaxed geometries (DA, D*A, DA* and $D^+A^-$), as calculated at the AM1-CI/COSMO level. The second charge transfer excited state (CT2) shown in Figure 2 will be discussed hereafter. The lowest excited state of the three-ring PPV oligomer is estimated to lie at 3.84 eV above the ground state, which is 0.3−0.4 eV higher than the experimental value in solution;[25] similary, the lowest electronic excitation of perylene bisimide is calculated at 2.8 eV to be compared to the experimental value of ∼2.5 eV.[26] In both cases, the excited state is mostly described by an electronic excitation between the HOMO and LUMO levels of the molecule. The AM1-CI approach thus appears to overestimate the optical transition energies; this behavior can be expected because (i) AM1 has been primarily parametrized to reproduce the geometric properties of molecules in their ground state and not their spectroscopic properties. However, because the charge transfer excited states globally originate from electronic transitions from occupied levels of the donor to unoccupied levels of the acceptor, the relative separation between the excited states, and hence the $\Delta G°$ values for charge generation, are expected to be well reproduced by our approach. In the cofacial geometry, the lowest charge transfer excited state is found to be almost isoenergetic with the lowest intramolecular excited state of PBI (assuming a dielectric constant of 3.5; see Methodology). This results in a driving force of −1.0 and +0.03 eV for the photoinduced electron and hole transfer, respectively. The energy difference between the ground state and the lowest charge transfer excited state (i.e., the driving force $\Delta G°$ for the charge recombination process) is estimated to be −2.84 eV; this value should be seen as an upper limit in view of the previous considerations.

Figure 3 depicts the changes in the bond lengths of the donor: (i) when going from D* to $D^+$ for the photoinduced electron transfer process, and (ii) when going from $D^+$ to D for the charge recombination and photoinduced hole transfer processes. Similar plots are presented for the acceptor when going from A to $A^-$ for the charge recombination and photoinduced electron transfer processes and from A* to $A^-$ for the photoinduced hole transfer. The results show that the geometric modifications are much less pronounced when going from an excited-state geometry to a charged geometry ($D^* \rightarrow D^+$ or $A^* \rightarrow A^-$) than between the ground state and a charged state. This translates into a $\lambda_i$ value of 0.19 eV (0 eV for PPV3 and 0.19 eV for PBI) for photoinduced electron transfer, 0.38 eV (0.35 eV for PPV3 and 0.03 eV for PBI) for photoinduced hole transfer, and 0.54 eV (0.35 eV for PPV3 and 0.19 eV for PBI) for charge recombination. For all processes, $\lambda_s$ is estimated to be 0.32 eV, as obtained from eq 3 with a static dielectric constant of 3.5.

The electronic coupling associated to the photoinduced electron transfer from D*A to CT1 is vanishingly small (on the order of 0.06 $cm^{-1}$) despite the fact that there is a significant *spatial* overlap between the two molecules. This can be rationalized in terms of the symmetry of the molecular orbitals involved in the process. Because CT1 is mostly described by an electronic transition from the HOMO of the donor to the LUMO of the acceptor and D*A by an electronic transition from the HOMO to the LUMO of the donor, the photoinduced electron transfer ($D^*A \rightarrow CT1$) can be seen globally in a one-electron picture as the transfer of one electron from the LUMO of the donor to the LUMO of the acceptor. The amplitude of the calculated electronic coupling can be rationalized either by analyzing the magnitude of the different parameters entering into eq 4 (in particular, the transition dipole moment) or simply, when the electron transfer mostly takes place between two electronic levels, by considering the degree of their electronic overlap that directly reflects the strength of the electronic coupling. Figure 4 shows the shape of the frontier electronic levels in PPV3 and PBI as well as their parity with respect to the center of inversion. Because the LUMO of the donor and acceptor units have opposite parities, there is full cancellation of bonding and antibonding interactions contributing to the global electronic overlap, thus rationalizing the small calculated electronic coupling.

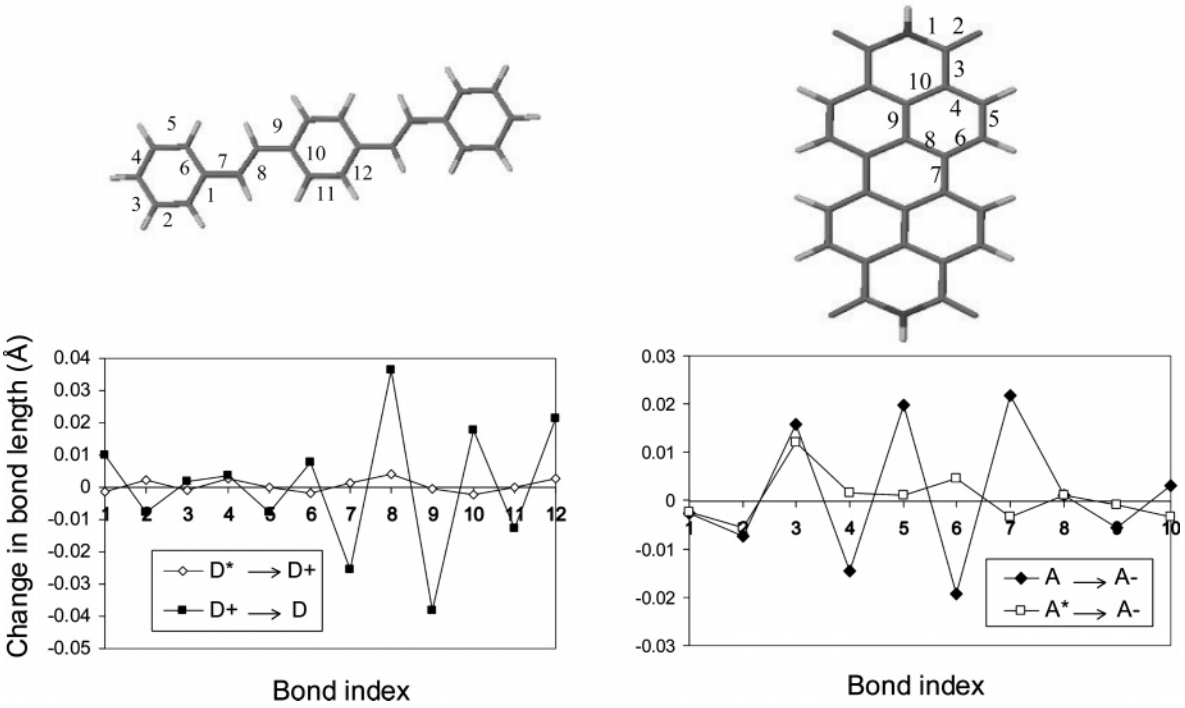


**Figure 3.** AM1-CI-calculated changes in the bond lengths in PPV3 associated with the D* → $D^+$ and $D^+$ → D transitions and in PBI for the A → $A^-$ and A* → $A^-$ transitions. The bond labeling is represented in the chemical structures on top of the graphs.

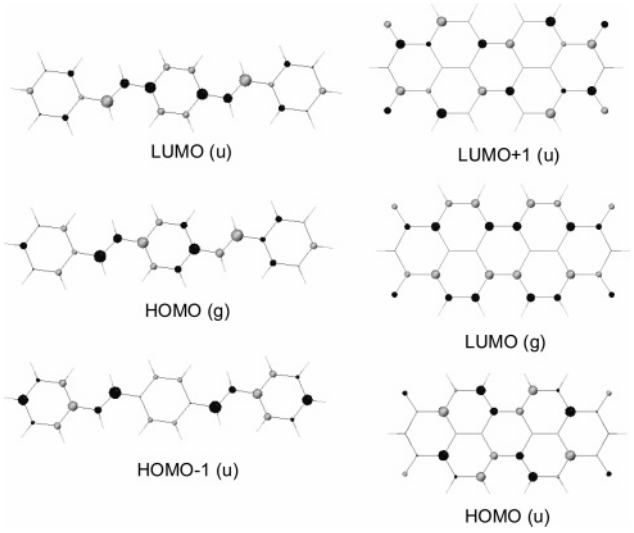


**Figure 4.** Representation of the shape of the frontier electronic levels of PPV3 (left) and PBI (right). The size and color of the balls reflect the amplitude and sign of the LCAO (linear combination of atomic orbitals) coefficients associated to the $p_z$ atomic orbitals.

Interestingly, the INDO/SCI calculations point to the existence of a second charge transfer excited-state lying 1.15 eV above the lowest charge transfer state. This state is described by the mixing of the H−1(D) → L(A) excitation (64%) and H(D) → L+1(A) excitation (36%). Note that the geometry of this excited charge transfer state cannot be readily optimized at the AM1-CI level; we thus assume in the following that CT2 is lying 1.15 eV above CT1 in the diagram shown in Figure 2, thus leading to a driving force of +0.15 and +1.18 eV for the photoinduced electron and hole transfer processes, respectively. We also stress that there is a third charge transfer state lying 0.71 eV above CT2; it is described by a mixing of the H−1(D) → L(A) excitation (36%) and H(D) → L+1(A) excitation (64%); this state is, however, too high in energy to be involved in the processes considered here. The electronic coupling between D*A and CT2 is significant (139 $cm^{-1}$) because there are no symmetry restrictions in this case. Indeed, the interaction between the H(D) → L(D) configuration, which mostly describes D*A, and the H(D) → L+1(A) contribution to CT2 implies an electron transfer from the LUMO of the donor to the LUMO+1 of the acceptor; the coupling is nonzero because these two levels have the same parity (see Figure 4). Similarly, the interaction between the H(D) → L(D) excitation and the H−1(D) → L(A) contribution to CT2 relies on the simultaneous transfer of the electron from the LUMO of the donor to the LUMO of the acceptor and the hole from the HOMO of the donor to the HOMO−1 of the same donor; this slightly contributes to the electronic coupling because the transition dipole moment between two configurations varying by more than two electrons is zero (the actual contribution actually arises from a small admixture of CT character in the D*A state of the complex).

Because the lowest excited state of PPV3 is lying at a higher energy than that of PBI, an energy transfer might take place from the donor to the acceptor prior the dissociation of the excitation via a photoinduced hole transfer. This is supported by experimental measurements performed in solution on supramolecular architectures linking covalently the donor and acceptor units.[13,27] When considering the photoinduced hole transfer process in our model complex, we calculate a vanishingly small electronic coupling (1.8 $cm^{-1}$) between the DA* and CT1 states. This process globally corresponds to the transfer of the hole from the HOMO of the acceptor to the HOMO of the donor; because these two levels have different parities, a small electronic is predicted, as is the case for the D*A → CT1 channel. When the excitation dissociation is initiated from the acceptor, CT2 turns out be too high in energy (1.18 eV above DA*) to yield an efficient dissociation pathway. We can thus conclude that charge generation via a photoinduced hole transfer is a very inefficient process in the highly symmetric arrangement of these two molecules.

That an excited charge transfer state has to be invoked to rationalize the full dynamics of exciton dissociation is consistent

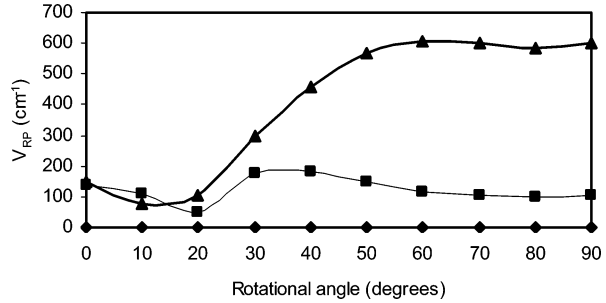


**Figure 5.** Evolution of the electronic coupling for the D*A → CT1 (filled diamonds), D*A → CT2 (filled squares) and $D^+A^-$ → DA (filled triangles) pathways as a function of the rotational angle in the PPV3/PBI complex, with an intermolecular distance fixed at 4 Å.

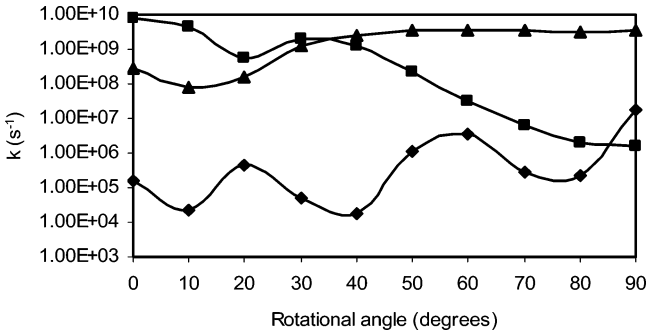


**Figure 6.** Evolution of the transfer rate for the D*A → CT1 (filled diamonds), D*A → CT2 (filled squares) and $D^+A^-$ → DA (filled triangles) pathways as a function of the rotational angle in the PPV3/PBI complex, with an intermolecular distance fixed at 4 Å.

with recent experimental data collected by Janssen and co-workers for tryad systems where two four-ring PPV oligomers are covalently attached to the terminal ends of a perylene bisimide derivative.[28] In this study, an energy transfer initially takes place from the PPV segment to the perylene bisimide and is followed by a photoinduced hole transfer via two dissociation pathways. A full theoretical analysis of the systems studied in ref 28 will be the subject of a subsequent publication. The implication of excited charge transfer states has also been evidenced experimentally in other donor/acceptor systems.[29,30]

For the charge recombination process, we can safely assume that it originates entirely from CT1 owing to the large energy difference between the lowest two charge transfer excited states. The charge recombination process globally results from the transfer of an electron from the LUMO of the acceptor to the HOMO of the donor. Because they have the same parity, the transfer is symmetry-allowed and characterized by a coupling of 149 $cm^{-1}$.

We are now in position to estimate the transfer rates of the three different electronic processes in our model complex, by injecting the different molecular parameters ($\Delta G°$, $\lambda_i$, $\lambda_s$, $V_{RP}$) in eq 1. Doing so, we obtain values of $1.31 \times 10^5$ and $9.12 \times 10^9$ $s^{-1}$ for the photoinduced electron transfer involving CT1 and CT2 (the same $\lambda_i$ and $\lambda_s$ values are assumed for the two states), respectively, $5.91 \times 10^6$ $s^{-1}$ for the photoinduced hole transfer, and $1.89 \times 10^8$ $s^{-1}$ for the charge recombination. The photoinduced electron transfer via CT1 and the charge recombination processes occur in the inverted Marcus region ($|\Delta G°| > \lambda$) whereas the other two processes take place in the normal region ($|\Delta G°| < \lambda$). The most efficient processes are the charge recombination and the photoinduced electron transfer via CT2, i.e., those for which the electronic coupling has a significant value. We also emphasize that the charge recombination rate increases up to $1.75 \times 10^9$ $s^{-1}$ when the driving force is reduced by 0.3 eV to artificially correct the AM1-CI/COSMO values.

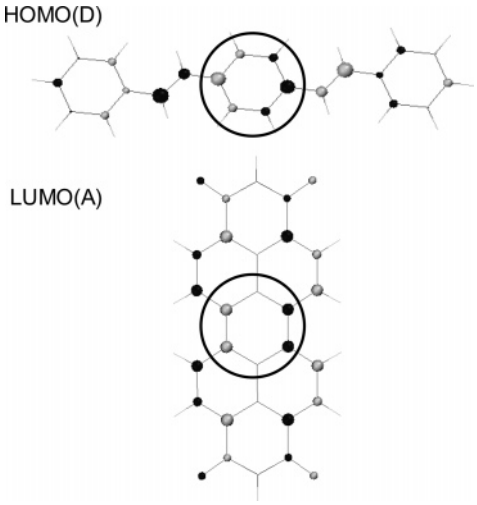


**Figure 7.** Illustration of the shape of the HOMO level of PPV3 and the LUMO level of PBI demonstrating the full antibonding interaction between the two levels in the overlapping region when the two molecules are rotated by 90°. The size and color of the balls reflect the amplitude and sign of the LCAO (linear combination of atomic orbitals) coefficients associated to the $p_z$ atomic orbitals.

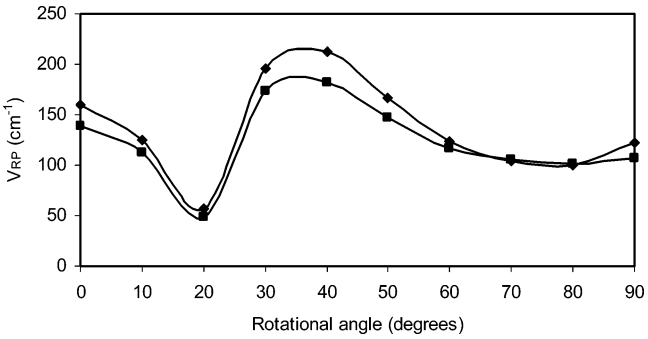


**Figure 8.** Evolution of the electronic coupling for the D*A → CT2 pathway, as calculated with the two-state GMH model with a CI expansion involving the 40 highest occupied levels and the 40 lowest unoccupied levels, with all the configurations originating from HOMO of the acceptor being eliminated (filled squares), and with only the configurations required to describe properly D*A and CT2 (filled diamonds).

The previous considerations hold true only for cofacial systems. We now analyze the way the photoinduced electron transfer and charge recombination rates are affected when modulating the relative position of the donor and acceptor units. In this context, we have first rotated the PPV3 oligomer on top of the perylene bisimide molecule from 0 to 90° while keeping their centers of mass exactly superimposed and the intermolecular distance at 4 Å. This operation hardly affects the driving force for charge recombination and photoinduced electron transfer via CT1 whereas the value associated to the CT2 pathway evolves from 0.12 to 0.35 eV going from 0 to 90°. This is explained by the fact that the HOMO−1 level of PPV3, involved in the latter process, displays an electron density localized over the external rings in contrast to the HOMO and LUMO levels; this pattern leads to a larger fluctuation of the Coulomb term when the rotational angle is varied, in contrast to the other processes. We report in Figure 5 the evolution of the electronic coupling associated to the three processes as a function of the rotational angle and the corresponding transfer rates in Figure 6.

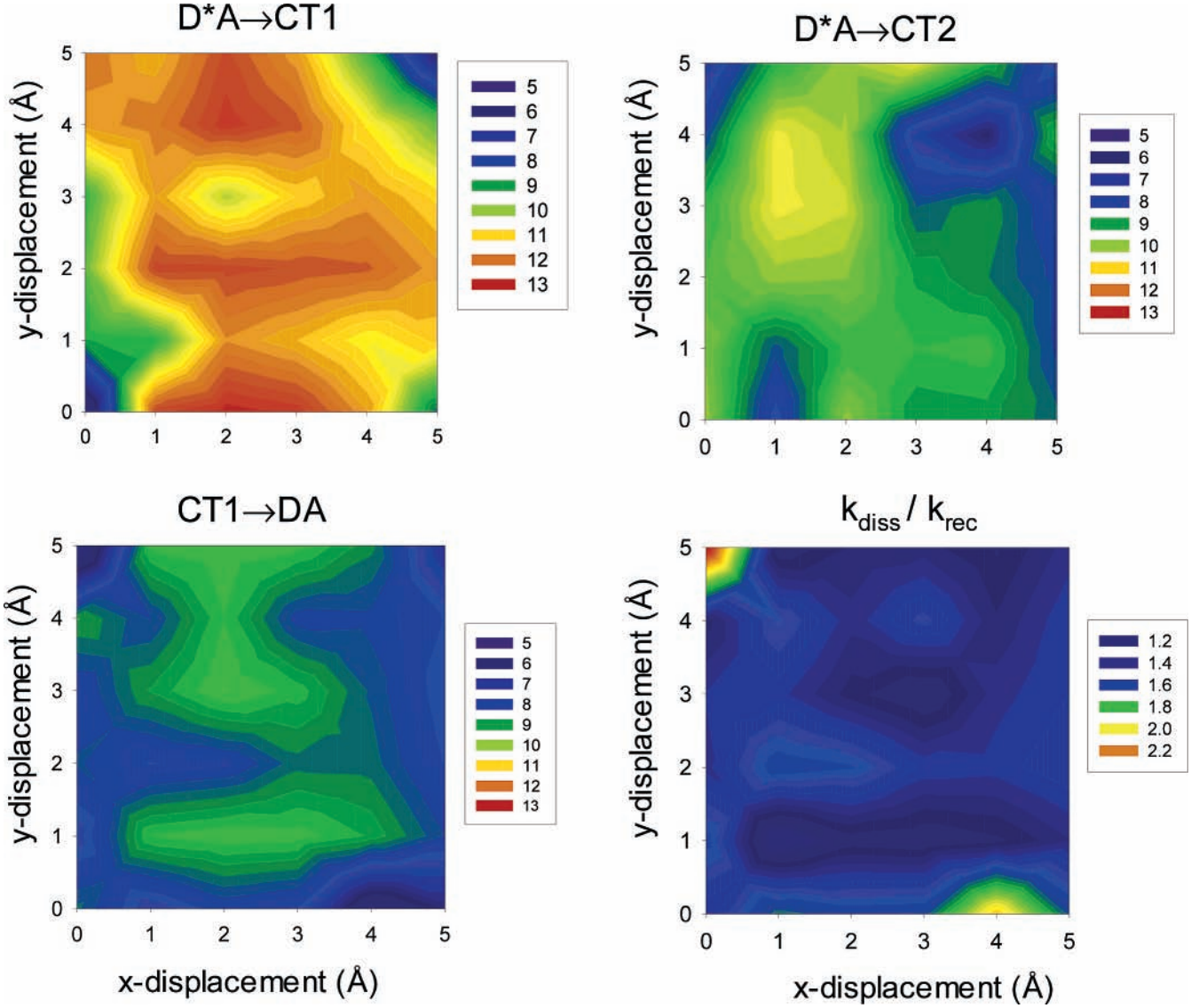


**Figure 9.** Evolution of the transfer rate for the D*A → CT1, D*A → CT2, and CT1 → DA when translating the PPV3 molecule by up to 5 Å along the positive *x* and/or *y* directions. The ratio between the rate calculated for charge generation (summing the two pathways) versus charge recombination is also displayed. The values appearing in the color scale correspond to the logarithm of the transfer rate (or transfer rate ratio).

The electronic coupling associated to the D*A → CT1 channel remains vanishingly small whatever the rotational angle, because the rotation does not break the symmetry constraints. The value for the D*A → CT2 pathway stays in the 100−200 $cm^{-1}$ range whereas a pronounced increase is observed for the recombination process from ∼100 $cm^{-1}$ to ∼600 $cm^{-1}$; the latter evolution is counterintuitive because one would expect a significant reduction in the electronic coupling when the spatial overlap gets reduced. This behavior has to be related once again to the shape of the HOMO(D) and LUMO(A) orbitals, as illustrated in Figure 7. When the angle is set to 90°, there is a full antibonding character between the two molecular wave functions in the whole overlapping region that leads to a large electronic coupling; in contrast, bonding and antibonding interactions are much more balanced at 0°, thus rationalizing why the electronic coupling is the largest at 90°. The evolution of the transfer rate with the rotational angle shows that the D*A → CT2 pathway is the fastest in the range between 0 and 40° whereas the recombination process governs the dynamics between 40 and 90°. We are thus led to the conclusion that some specific configurations obtained upon *rotation* could prove highly detrimental for the efficiency of organic solar cells.

We have validated at this stage the use of the two-state GMH formalism by plotting in Figure 8 the evolution of the rate for the D*A → CT2 pathways as a function of the angle when (i) using a CI expansion involving the 40 highest occupied levels and the 40 lowest unoccupied levels, with all the configurations originating from HOMO(A) being eliminated, and (ii) involving only the configurations required to describe properly D*A and CT2. The similarity between the two sets of data fully supports the choice of a two-state model. The same conclusions are reached for the D*A → CT1 and $D^+A^-$ → DA channels. We have further checked the stability of our calibration procedure by tuning the location of the CT2 state over a range of 1 eV. The electronic coupling associated to the D*A → CT2 channel in the cofacial geometry are found to evolve from 150 to 250 $cm^{-1}$; this translates into changes in the transfer rates by only a factor of 3.

Finally, we have translated the PPV oligomer on top of the perylene bisimide molecule along both the *x* and *y* axes, as defined in Figure 2. The two-dimensional grids shown in Figure 9 display the transfer rates for the three processes when shifting the PPV oligomer by up to 5 Å in the positive *x* and/or *y* directions. The rates have been computed for 36 different

configurations by keeping $\Delta G°$ and $\lambda_s$ equal to the values obtained for the ($x = 0$, $y = 0$) dimer and by recalculating $V_{RP}$ for each configuration, with the lowest charge transfer state (CT1) positioned at the same energy as in the cofacial dimer. The results show that the D*A → CT1 pathway becomes more efficient than D*A → CT2 when going away from the ($x = 0$, $y = 0$) complex; the translation actually leads to a breaking of the symmetry constraints imposed to D*A → CT1 in the highly symmetric arrangement and promotes a large electronic coupling for this channel. The ratio calculated for the rate of charge generation (summing the two different pathways) versus charge recombination is typically about 1 order of magnitude. This indicates that small *translations* do not promote geometric configurations that would prevent good device performance.

## 4. Conclusions

We have calculated the rates for charge generation and recombination in model complexes built from a three-ring PPV oligomer as donor and bisimide as acceptor. This has been achieved by calculating at the semiempirical Hartree−Fock level the various parameters entering into the rate, as expressed within the Marcus−Levich−Jortner formalism. The results show that (i) a dissociation pathway involving an excited charge transfer state has to be taken into account to fully rationalize the dynamics of the charge generation process; the number of charge transfer states to be considered is expected to grow with the molecular size of the donor and/or acceptor; (ii) there is no direct relationship between the degree of spatial overlap between the two molecules and the amplitude of the electronic coupling; (iii) the amplitude of the electronic coupling is governed by symmetry considerations in highly symmetric arrangements; and (iv) the transfer rate is found to be larger for the charge recombination than for the charge generation process in some specific configurations, thus proving highly detrimental for the solar cell. These calculations provide guidelines to synthetic chemists for the design of the best matching partners and the best supramolecular architectures for organic solar cells.

**Acknowledgment.** We acknowledge very stimulating discussions with Prof. R. A. J. Janssen. The work in Mons is partly supported by the Belgian Federal Governement "Interuniversity Attraction Pole in Supramolecular Chemistry and Catalysis, PAI 5/3", the Région Wallonne (Program PIMENT-SOLPLAST), the European Integrated Project project NAIMO (NMP4-CT-2004-500355), and the Belgian National Fund for Scientific Research (FNRS/FRFC). J.C. and D.B. are FNRS Research Associates; V.L. acknowledges a grant from "Fonds pour la Formation à la Recherche dans l'Industrie et dans l'Agriculture (FRIA)".

## References and Notes

(1) Sariciftci, N. S.; Smilowitz, L.; Heeger, A. J.; Wudl, F. *Science* **1992**, *58*, 1474.
(2) Brabec, C. J.; Sariciftci, N. S.; Hummelen, J. C. *Adv. Funct. Mater.* **2001**, *11*, 15.
(3) http://solar-club.web.cern.ch/solar-club/Futur/PVnews.html.
(4) Winder, C.; Sariciftci, N. S. *J. Mater. Chem.* **2004**, *14*, 1077.
(5) Jayakannan, M.; Van Hal, P. A.; Janssen, R. A. J. *J. Polym. Sci. Polym. Chem.* **2002**, *40*, 2360.
(6) Perepichka, I. F.; Levillain, E.; Roncali, J. *J. Mater. Chem.* **2004**, *14*, 1679.
(7) Thomas, C. A.; Zong, K. W.; Abboud, K. A.; Steel, P. J.; Reynolds, J. R. *J. Am. Chem. Soc.* **2004**, *126*, 16440.
(8) Henckens, A.; Colladet, K.; Fourier, S.; Cleij, T. J.; Lutsen, L.; Gelan, J.; Vanderzande, D. *Macromolecules* **2005**, *38*, 19.
(9) Halls, J. J. M.; Pichler, K.; Friend, R. H.; Moratti, S. C.; Holmes, A. B. *Appl. Phys. Lett.* **1996**, *68*, 3120.
(10) Halls, J. J. M.; Cornil, J.; dos Santos, D. A.; Silbey, R.; Hwang, D. H.; Holmes, A. B.; Brédas, J. L.; Friend, R. H. *Phys. Rev. B* **1998**, *60*, 5721.
(11) Lemaur, V.; Steel, M.; Beljonne, D.; Brédas, J. L.; Cornil, J. *J. Am. Chem. Soc.* **2005**, *127*, 6077.
(12) Neuteboom, E. E.; vanHal, P. A.; Janssen, R. A. J. *Chem. Eur. J.* **2004**, *10*, 3907.
(13) Würthner, F.; Chen, Z.; Hoeben, F. J. M.; Osswald, P.; You, C. C.; Jonkheijm, P.; Herrikhuyzen, J. V.; Schenning, A. P. H. J.; van der Schoot, P. P. A. M.; Meijer, E. W.; Beckers, E. H. A.; Meskers, S. C. J.; Janssen, R. A. J. *J. Am. Chem. Soc.* **2004**, *126*, 10611.
(14) Neuteboom, E. E.; Meskers, S. C. J.; van Hal, P. A.; van Duren, J. K. J.; Meijer, E. W.; Janssen, R. A. J.; Dupin, H.; Pourtois, G.; Cornil, J.; Lazzaroni, R.; Brédas, J. L.; Beljonne, D. *J. Am. Chem. Soc.* **2003**, *125*, 8625.
(15) Barbara, P. F.; Meyer, T. J.; Ratner, M. A. *J. Phys. Chem.* **1996**, *100*, 13148.
(16) Dewar, M. J. S.; Zoebisch, E. G.; Healy, E. F.; Stewart, J. J. P. *J. Am. Chem. Soc.* **1985**, *107*, 3902.
(17) We have used the AMPAC package, with a size of the active space chosen in all instances so as to ensure the convergence of the results.
(18) Klamt, A.; Schürmann, G. *J. Chem. Soc., Perkin Trans.* **1993**, *2*, 799.
(19) Brocks, G.; van den Brink, J.; Morpurgo, A. F. *Phys. Rev. Lett.* **2004**, *93*, 146405.
(20) Cornil, J.; Beljonne, D.; Coropceanu, V.; Brédas, J. L. *Chem. Rev.* **2004**, *104*, 4971.
(21) Marcus, R. A. *J. Chem. Phys.* **1965**, *43*, 679.
(22) Cave, R. J.; Newton, M. D. *Chem. Phys. Lett.* **1996**, *249*, 15.
(23) Nelsen, S. F.; Newton, M. D. *J. Phys. Chem. A* **2000**, *104*, 10023.
(24) Ridley, J.; Zerner, M. C. *Theor. Chim. Acta* **1973**, *32*, 111.
(25) Schenk, R.; Gregorius, H.; Müllen, K. *Adv. Mater.* **1991**, *3*, 492.
(26) Offermans, T.; Meskers, S. C. J.; Janssen, R. A. J. *J. Chem. Phys.* **2003**, *119*, 10924.
(27) Beckers, E. H. A.; van Hal, P. A.; Schenning, A. P. H. J.; Elghayoury, A.; Peeters, E.; Rispens, M. T.; Hummelen, J. C.; Meijer, E. W.; Janssen, R. A. J. *J. Mater. Chem.* **2002**, *12*, 2054.
(28) Beckers, E. H. A.; Meskers, S. C. J.; Schenning, A. P. H. J.; Chen, Z.; Würthner, F.; Janssen, R. A. J. *J. Phys. Chem. B* **2004**, *108*, 6933.
(29) Sautter, A.; Kaletas, B. K.; Schmid, D. G.; Dobrawa, R.; Zimine, M.; Jung, G.; van Stokkum, I. H. M.; De Cola, L.; Williams, R. M.; Würthner, F. *J. Am. Chem. Soc.* **2005**, *127*, 6719.
(30) Prodi, A.; Chiorboli, C.; Scandola, F.; Iengo, E.; Alessio, E.; Dobrawa, R.; Würthner, F. *J. Am. Chem. Soc.* **2005**, *127*, 1454.